Published in final edited form as:
Lasers Med Sci. 2013 September ; 28(5): 1315–1321. doi:10.1007/s10103-012-1235-8.

Investigation on safety aspects of forward light propagation during laser surgery

Hyun Wook Kang,
Department of Biomedical Engineering, Pukyong National University, 45 Yongso-ro, Nam-gu, Busan 608-737, South Korea

Jeehyun Kim, and
School of Electrical Engineering and Computer Science, Kyungpook National University, 1370 Sankyuk-dong, Buk-gu, Daegu 702-701, South Korea

Junghwan Oh
Department of Biomedical Engineering, Pukyong National University, 45 Yongso-ro, Nam-gu, Busan 608-737, South Korea

Jeehyun Kim: jeehk@knu.ac.kr; Junghwan Oh: jungoh@pknu.ac.kr

Abstract

During laser treatment of prostate, urological surgeons occasionally experience fiber-cap failure due to concentration of thermal stress on the fiber tip. Upon the cap breakage, laser light becomes forward-propagating and may adversely affect the bladder tissue such as perforation. The purpose of the current study was to identify any bladder perforation with forward-propagating laser light (λ = 532 nm) at 80 and 120 W with an assumption of fiber-cap failure. Perforation time was measured and compared in terms of fiber distance. The results showed that 80 and 120 W perforated the tissue up to 2 and 2.5 cm, respectively with perforation threshold of 17.2 kW/cm^2, and the minimum perforation time was approximately 7 s. No perforation occurred at the distance of 3 cm for 1-min irradiation at both power levels, but severely carbonized lesions were generated around the irradiated tissue. Although equivalent ablation speed was found between the two power levels, 120 W created up to 20 % wider craters regardless of fiber distance. With consideration of dense collagen fibers in bladder structure and long surgical distance, direct incidence of laser perforation on bladder wall could be unlikely to happen upon fiber-cap failure during laser surgery.

Keywords

Ablation; Bladder wall; Carbonization; Laser perforation

Introduction

Among various wavelengths, visible 532 nm and mid-IR 2.12 μm have primarily been used for laser therapy to treat urological diseases such as stricture, benign prostatic hyperplasia, condyloma, and kidney stone [1–4]. Although Nd: YAG (1,064 nm) lasers were often used for urological applications [5, 6], their long optical penetration depth caused deep thermal injury in soft tissue and thus curtailed their clinical applications [7]. Both 532-nm and 2.12-μm wavelengths are typically delivered through a 600- μm core or smaller optical fiber

Correspondence to: Jeehyun Kim, jeehk@knu.ac.kr; Junghwan Oh, jungoh@pknu.ac.kr.

during laser treatment, but they have different optical responses in tissue. In the case of the mid-IR 2.12 μm, as the major chromophore is water, the wavelength can treat a variety of soft tissues. According to Beer's law, the wavelength due to its high absorption coefficient (μ_a=26 cm^{-1}) can also lose 67 % of the optical energy within even a 400-(μm thick water layer in between fiber tip and target tissue under aqueous environment [8]. However, this energy loss can be a precaution against misdirected laser irradiation. On the other hand, the visible 532-nm wavelength is exclusively absorbed by oxy-hemoglobin, and it can readily ablate or coagulate vascularized tissues, for instance, blood vessels under the skin, prostate, and kidney [9, 10]. Due to optical characteristics, the visible light can easily penetrate water environment with negligible light absorption [11].

During 532-nm laser therapy, a side-firing fiber is often used to deliver laser light in order to treat tubular geometry of the urinary tissue [2, 9, 10]. Since beam size on the tip surface is small (approximately 0.3 mm^2), the fiber tip experiences local thermal stress due to debris accumulation on the tip during laser ablation [12, 13]. If the concentrated stress is beyond tolerable mechanical strength of the protective glass cap on the tip, it is hard to avoid thermally induced damage to the cap, glass devitrification, and its eventual failure at the rate of up to 12 % in clinical situations [13]. One of the clinical concerns pertaining to the fiber-tip breakage is undesirable thermal damage to the peripheral tissue. For example, during laser prostatectomy, the fiber failure allows the light out of the fiber tip to propagate forward and to detrimentally interact with the bladder tissue in front. Depending upon the interaction time and/or physical distance, the tissue may undergo severe thermal stress, leading to puncture of the urinary bladder wall and eventually bladder failure. Farag's group reported a clinical case of bladder perforation in association with laser ablation of the prostate [14]. In addition, Hermann's group quantitatively demonstrated the deterioration of the fiber tip as well as fiber failure during laser surgery, possibly leading to irreversible damage to the surrounding tissue [12, 13]. However, photothermal effect in the bladder tissue during laser surgery is still poorly understood.

In the current study, we investigated the ablative effect of forward-propagating laser light on bladder tissue in terms of safely aspects during clinical laser prostatectomy. The purpose of our study was to verify any detrimental effect of forward beam propagation on the tissue upon fiber-cap failure and to characterize potential tissue perforation at various fiber distances and irradiation times under two power levels frequently used for laser surgery. Post-experimentally, thermal injury to tissue induced by laser irradiation was quantitatively examined in light of ablation speed, irradiance, and coagulative necrosis in order to understand the clinical implications.

Materials and methods

Sample preparation

Bovine urinary bladder tissue was utilized as a tissue model to evaluate thermal response of tissue to laser irradiation. The tissue samples were obtained from a local slaughter house 4 h after animal euthanasia and were stored at 4 °C for 24 h prior to experiments. A total of 100 samples were cut in a size of approximately 4×4 cm^2 to achieve a flat surface of the bladder wall, so the laser light was perpendicularly irradiated to the surface. Prior to the tests, each tissue sample was placed in a transparent sample chamber and slightly thinned out in between two metal plates of a tissue holder (Fig. 1). The thickness of the sample was uniformly maintained at around 4.5 mm, which is the typical thickness of the detrusor layer of the bladder [15]. Then, the chamber was filled with saline to mimic a clinical situation (Fig. 1). After irradiation, all the irradiated tissues were fixed in 10 % buffered formalin and evaluated in terms of ablated crater size, perforation time, and thermal coagulation zone size as a function of fiber distance between the fiber tip and tissue surface.

Experimental setup

A conventional surgical laser (λ =532 nm, τ_p=100 ns at FWHM, and repetition rate=20 kHz, high performance system, Laserscope, CA, USA) was employed as a light source for our in vitro study. Two power levels (80 and 120 W), which are frequently used for laser prostatectomy, were evaluated with bladder tissue. In order to deliver laser energy, a 600-μm quartz end-firing fiber with NA=0.22 (ADD Stat, Laserscope) was utilized, emulating a situation of forward light propagation after probable fiber-cap failure. In other words, the glass cap at the distal tip of a side-firing fiber used for laser surgery was removed and mechanically polished to transmit the laser light straight out of the fiber tip. Transmission (%) of the fiber was measured with a power meter (Nova II, Ophir-Spiricon, North Logan, UT, USA) before and after each ablation test to maintain transmission variations within 5 % and to minimize debris contamination to the fiber transmission. Due to light divergence, the beam spot size ($1/e^2$) out of the fiber was pre-experimentally measured with a beam profiler (Pyrocam II, Ophir-Spiricon) at various distances from 0 to 10 cm with an increment of 1 cm under both power levels. The measured beam spot size (mm) was then used to calculate the corresponding irradiance (I= applied power/calculated beam area, kW/cm^2) at each fiber distance.

Figure 1 shows a detailed illustration of the experimental setup. The fiber was initially inserted into a 23 Fr cystoscope (23 Fr urethrocystoscope, Karl Storz, Germany) that is typically used for clinical situations, and saline was supplied to the inlet of the cystoscope (Fig. 1). Then, the cystoscope was vertically attached to a translational stage and moved along the z-axis to vary the physical distances between the fiber tip and the tissue surface from 0.5 to 3 cm with an increment of 0.5 cm. Prior to each ablation test, a sample chamber was filled with saline (maintained at room temperature) to completely submerge the tip of the cystoscope. After the test, the chamber was emptied and then refilled with fresh saline to eliminate residual-debris contamination in the chamber. A constant saline flow at the rate of 6.9 ml/s was applied to the fiber tip at the outlet of the cystoscope (Fig. 1), and the flow prevented any ablated debris from re-attaching to the tip and contaminating the irradiated area on the tissue and cooled down both the tip and tissue surface during the tissue ablation. The temperature of the saline was monitored before and after each test to maintain it at room temperature. A photodetector with a lens was set up next to the tissue chamber (Fig. 1) in order to selectively detect any scattered photons penetrating through the tissue (if perforated) and to identify the onset of tissue perforation (i.e., no unscattered transmitted photons were detected). Tissue perforation was defined as the moment when the photodetector sensed any light signal coming through the perforated bladder tissue. Laser was irradiated on the tissue for up to 3 min unless perforation occurred, but upon perforation, laser irradiation stopped immediately. Laser-induced tissue perforation time was measured and recorded with two different power levels (80 and 120 W) at various fiber distances. Ten specimens were used for each distance condition (N=10), and each specimen was fixed in formalin after the ablation test. For safety purposes, the bottom of the chamber was made of a piece of black metal to dump the residual light that could penetrate the target tissue.

For post-experimental analysis, each formalin-fixed tissue was cut in half along the center of the laser-induced craters and imaged by a digital camera. Then, the thickness of each sample, crater dimension (width and depth), and coagulative necrosis were estimated by means of image analysis software (Image J, National Institute of Health, MD, USA) after calibration. In this study, the crater width was defined as the maximum lateral distance at the crater top surface, and the acute coagulation zone was defined as the region with discoloration along the crater wall [16]. The coagulation zone was measured at five different locations around each crater (3, 4, 5, 6, and 9 o'clock). Student's t test (two-tailed) was used to perform statistical analysis, and $p< 0.05$ means statistically significant.

Results

Figure 2 presents top and cross-sectional images of the bladder tissue perforated with 120 W at various fiber distances. Evidently, the bladder-wall perforation took place at the distance of up to 2 cm, but no perforation was observed at 3-cm distance even for 1-min irradiation. In the case of relatively higher irradiances at 0.5 and 1 cm distances (I= 35.7 and 32.3 kW/cm^2), the drilled holes were uniformly created with partial carbonization (less than 100 μm thick) and relatively thin coagulation (0.49±0.09 mm), as shown in Fig. 2a, b. However, further distance of 2 cm associated with lower irradiance (I=23.4 kW/cm^2) still perforated the bladder tissue along with a carbonized ring (around 0.75 mm thick on the surface) around the crater and thicker coagulation necrosis (0.75 ±0.23 mm), as shown in Fig. 2c. It was noted that the shape of the crater bottom became narrower, and the bottom of the tissue was slightly deformed due to excessive thermal denaturation (Fig. 2c). At 3 cm with 18.3 kW/cm^2, the tissue was superficially ablated (~1.5 mm) but left excessively carbonized lesion (up to 1 mm thick on the surface) and thick coagulation necrosis (1.06±0.17 mm) on the crater wall (Fig. 2d). Carbonized debris even covered the entrance of the ablated area (top view in Fig. 2d). Similar perforation trends were also observed with 80 W up to 1.5-cm distance.

Figure 3 shows laser-induced perforation time (left axis) and corresponding irradiance on tissue surface (right axis) simultaneously as a function of fiber distance at two power levels. Black circles (hollow for 80 W and solid for 120 W) correspond to the data for perforation time on the left axis, and blue squares (hollow for 80 W and solid for 120 W) represent the data for the calculated irradiance on the right axis. The dotted lines (blue for irradiance and red for perforation time) represent the tendency of each data group with respect to variations in fiber distance. Based upon the perforation time, the total energy applied can be calculated by multiplying the applied power with the perforation time. Thus, at 80 W, the energy applied was 523, 667, 854, and 1,904 J at 0.5, 1, 1.5, and 2 cm, respectively. At 120 W, the energy applied was 862, 1,042, 1,276, 2,722, and 3,956 J at 0.5, 1, 1.5, 2, and 2.5 cm, respectively. Both 80 W (hollow black circle) and 120 W (solid black circle) demonstrated that the perforation time increased rapidly with the fiber distance, and irrespective of the applied power, almost equivalent perforation times were observed up to 2-cm distance. Nevertheless, at 2.5-cm distance, 120 W was still able to perforate the tissue, whereas 80 W merely ablated a superficial layer of the bladder tissue. Eventually, neither power levels perforated the tissue at 3-cm distance. On the other hand, as the measured beam spot size increased, the corresponding irradiance at 80 W (blue hollow square) and 120 W (blue solid square) exponentially decreased with the fiber distance. On account of the applied power level, there was always 50 % difference in irradiance between 80 and 120 W. In Fig. 3, the perforation threshold, defined by the irradiance to complete tissue perforation, was found to be 17.2 kW/cm^2 (i.e., irradiance at 80 W and 2-cm distance). In case of 2.5-cm distance, the corresponding irradiance at 80 W ($I_{80\ w}$= 15.2 kW/cm^2) was lower than the perforation threshold. On the other hand, the irradiance at 120 W ($I_{120\ w}$=20.8 kW/cm^2) was still above the threshold of 17.2 kW/cm^2, but at 3-cm distance, $I_{120\ w}$ became near-threshold (i.e., 18.1 kW/cm^2). Table 1 summarizes the perforation speed comparison as a function of fiber distance between 80 and 120 W.

Thermal response of the bladder tissue at 3 cm was also examined with 80 and 120 W. Figure 4 shows top and cross-sectional images of the irradiated bladder tissue. Both cases demonstrated shallower tissue ablation in the middle (i.e., no perforation) along with excessive carbonization on the rim as well as crater wall. From the cross-sectional images, coagulative necrosis regions (discolored area) were visually observed, surrounding the ablated crater. The coagulation zone at 120 W was approximately 26 % thicker than that at 80 W (1.06±0.17 mm vs. 0.84±0.15 mm, respectively; p< 0.005 and N=6). In order to

validate the beam-spot changes at various distances, laser-induced crater width in the bladder tissue was also measured and compared between 80 and 120 W (Fig. 5). Overall, the crater width (i.e., 2.8 mm at 120 W and 0.5 cm) was much larger than the spot size (around 1 mm at 0.5 cm) due to lateral heat conduction instrumental in augmenting tissue removal. For the current study, it was assumed that intrinsic tissue properties (optical, thermal, and mechanical) were almost equivalent, and the only variables to change the crater geometry would be fiber distance and applied power; in turn, the crater width could reflect the effect of light divergence on tissue at various distances and two power levels. Regardless of power, the crater width initially remained constant up to 1-cm distance but rapidly increased with the fiber distance. Due to higher light intensity, 120 W created up to approximately 20 % wider craters than 80 W regardless of fiber distance ($p < 0.001$ and $N=5$).

Discussion

Photothermal response of the bladder tissue was evaluated to identify any probable adverse effect of forward light propagation on clinical outcomes during laser surgery. According to the current results, fiber distance was demonstrated to be the critical element to determine laser-induced tissue perforation in this study as the beam spot size on the tissue surface concomitantly changed due to beam divergence (Fig. 3). Thus, the degree of the perforation time variation was correlated with the applied irradiance under two power levels (Fig. 3). Figure 2c also exhibited that the geometry of the ablation craters altered and became narrower with the fiber distance, possibly due to the decreasing irradiance along z-axis. However, further investigations will be necessary to confirm the effect of irradiance on ablation geometry. The maximum distance for laser-induced perforation was contingent upon the applied power level and beam spot size (i.e., 2 cm for 80 W, and 2.5 cm for 120 W). The perforation threshold at 17.2 kW/cm^2 (i.e., irradiance at 80 W and 2-cm distance) overtly confirmed the degree of tissue perforation, in that the irradiance sub- ($I_{80\ w}$=15.2 kW/cm^2 at 2.5 cm) or near-threshold ($I_{120\ w}$= 18.1 kW/cm^2 at 3 cm) was insufficient to complete tissue drilling, leading to no perforation.

In an attempt to complete tissue perforation in the current study, both 80 and 120 W required the minimum time of approximately 7 s (at 0.5-cm distance), which is longer than the time to perforate porcine kidney tissue (5 mm thickness perforated in 4.2 s at 120 W [17]). Typically, bladder tissue is composed of connective tissue matrix and collagen fibers, whereas kidney tissue is mostly glandular and hemoglobin-rich [15, 17]. Thus, stronger mechanical structure as well as relatively lower light absorption of the bladder tissue might have prolonged tissue perforation. In addition, to understand the effect of power on tissue perforation process as a function of time, laser-induced perforation speed was calculated and compared in Table 1. Both power levels showed decreasing perforation speed with increasing fiber distance. In spite of the different power levels, the perforation speed was quite comparable up to 2-cm distance ($p>0.05$). This phenomenon can be explained in part by spatial distribution of light intensity. Although the overall beam distribution at both power levels would be a Gaussian profile, it was likely that the spatial beam distribution at 120 W became more widely distributed but with the peak intensity of the beam center similar to that of 80 W. In fact, Fig. 5 exhibited that the crater width at 120 W increased by up to 20 % in comparison with 80 W. Therefore, comparable speeds of axial ablation as well as different crater widths could implicate that the light intensity of the beam center hardly or slightly changed, but the wing parts of the beam profile increased sufficiently (above the ablation threshold) to augment lateral tissue ablation. Aforementioned in the “Materials and methods” section, the thickness of the bladder specimens was consistently maintained at approximately 4.5 mm in order to minimize tissue variations and to reflect the thickness of the detrusor layer of the bladder [15]. However, intrinsic structure of the tissue is typically inho-mogeneous, which might have influenced the perforation process and could explain the

variations in perforation time (Fig. 3). Additional experiments are underway to confirm the current hypothesis by comparing spatial beam profiles under 80 and 120 W at various distances up to 3 cm with a 3-D beam profiler.

At 3 cm, both tested power levels were unable to perforate bladder tissue due to sub- or near-threshold irradiance (i.e., I_{th}= 17.2 kW/cm^2) under the current study. As shown in Fig. 4, the craters produced at 80 and 120 W accompanied a severe carbonization rim around the ablated spot as a result of excessive heat accumulation. Besides, constant heating even for 1 min at sub- or near-threshold was possibly responsible for peripheral tissue charring. As fiber distance increased, resultantly lowered irradiance merely heated up the tissue surface. The elapse of long irradiation time at the sub-threshold ultimately induced local surface ablation and significantly developed carbonization on the tissue surface. As the carbonized (black) tissue serves typically as an absorber for the incident optical energy, the formation of charring subsequently heated up the irradiated tissue and then generated coagulation necrosis in the tissue (Fig. 2) rather than progressing tissue ablation; thus, carbonized necrosis was continuously aggravated with irradiation time. Both sub-threshold irradiance and light absorption by carbonized tissue could, thereby, have prohibited the laser-induced perforation of bladder wall at 3-cm distance.

The current in vitro tests demonstrated that under 120-W application, bladder perforation could take place after approximately 7-s irradiation at 0.5-cm distance and longer than 30 s at 2.5 cm; however, no perforation was induced at 3-cm distance even for 1-min irradiation. Based upon clinical laser procedures, the actual distance between the distal portion of bladder wall and the fiber tip could be longer than 3 cm, and bladder distention might increase the distance even further. In spite of forward light propagation due to undesirable cap failure, bladder perforation was mostly related to irradiation with a fresh fiber (no cap failure) on 1–2-mm thin bladder neck [14, 18] or misfiring while rubbing the fiber against the bladder tissue [19, 20]. Thus, proper techniques as well as training have been emphasized along with technical recommendations to prevent any adverse tissue perforation event [20, 21]. In addition, in man, the thickness of the urinary bladder wall is approximately 5.7 mm with respect to the three different layers: urothelium (cell layers), lamina propia (1.3-mm thick connective tissue matrix), and detrusor layer (4.4-mm thick smooth muscle) [15]. Therefore, it is conceivable that thicker structure prevents human bladder wall from being readily perforated with forward-propagating laser light unless the tissue is irradiated for a long period of time and/or at a very close distance. In fact, irradiating light on a single spot for 7 s is too long for surgeons to be inattentive during laser surgery. There may, however, be thermally induced irreversible alterations of proteins and other biological molecules, cells, and extracellular components in the tissue as a result of continuous heating. Accordingly, these alterations will be verified in the follow-up in vivo studies with the aim of revealing any photothermal injury leading to possible bladder failure.

Conclusion

Laser-induced perforation in the urinary bladder wall was quantitatively evaluated for safety purposes. Both 80 and 120 W perforated the tissue up to 2 cm at an equivalent ablation speed, but 120 W still drilled the tissue at even further distance of 2.5 cm due to higher irradiance. At 3 cm, neither power levels perforated the target tissue but entailed significant carbonization on the crater surface, resulting from excessive heat accumulation. Sub-threshold irradiance as well as undesirable light absorption by carbonized tissue could have prohibited the progress of tissue perforation at 3 cm. Comparable perforation speed and different crater widths implied that the beam profile at 120 W could be more widely distributed with comparable peak intensity to that of 80 W, eventually augmenting lateral tissue ablation. In clinical situations, it would be more difficult to perforate the bladder due

to 3-cm or longer surgical distance between the fiber tip and the tissue, and thick bladder tissue layer with dense collagen fibers. Therefore, the current results demonstrated that the immediate occurrence of detrimental perforation on urinary bladder wall after fiber failure during laser surgery might be unlikely.

Acknowledgments

This study was financially supported by the Ministry of Health and Welfare, Republic of Korea through the Korea Healthcare Technology R&D Project (A102024-1011-0000200), Business for Cooperative R&D between Industry, Academy, and Research Institute funded by the Korea Small and Medium Administration in 2012 (grant no.: C0018575), and National Institutes of Health (NIBIB, R01 EB013723, S.A.B.).

References

1. Pierre SA, Albala DM. The future of lasers in urology. World J Urol. 2007; 25:275–283. [PubMed: 17569055]
2. Pereira-Correia JA, de Moraes Sousa KD, Santos JB, et al. GreenLight HPS 120-W laser vaporization vs transurethral resection of the prostate (<60 mL): a 2-year randomized double-blind prospective urodynamic investigation. BJU Int. 201210.1111/j.1464-410X.2011.10878.x
3. Choi SW, Choi YS, Bae WJ, et al. 120 W Greenlight HPS laser photoselective vaporization of the prostate for treatment of benign prostatic hyperplasia in men with detrusor underactivity. Korean J Urol. 2011; 52:824–828. [PubMed: 22216394]
4. Cornu JN, Terrasa JB, Lukacs B. Ex-vivo comparison of available morcellation devices during holmium laser enucleation of the prostate through objective parameters. J Endourol. 201210.1089/end.2011.0454
5. Rothenberger K, Pensel J, Hofstetter A, et al. Transurethral laser coagulation for treatment of urinary bladder tumors. Lasers Surg Med. 1983; 2:255–260. [PubMed: 6687747]
6. Pensel J. Dosimetry of the neodymium-YAG laser in uro-logical applications. Eur Urol. 1986; 12(Suppl 1):17–20. [PubMed: 3770022]
7. Kuntzman RS, Malek RS, Barrett DM, et al. Potassium-titanyl-phosphate laser vaporization of the prostate: a comparative functional and pathologic study in canines. Urology. 1996; 48:575–583. [PubMed: 8886063]
8. Chan KF, Vassar GJ, Pfefer TJ, et al. Holmium:YAG laser lithotripsy: a dominant photothermal ablative mechanism with chemical decomposition of urinary calculi. Lasers Surg Med. 1999; 25:22–37. [PubMed: 10421883]
9. Malek RS, Kang HW, Coad JE, Koullick E. Greenlight photoselective 120-watt 532-nm lithium triborate laser vaporization prostatectomy in living canines. J Endourol. 2009; 23:837–845. [PubMed: 19371169]
10. Malek RS, Kang HW, Peng YS, et al. Photoselective vaporization prostatectomy: experience with a novel 180 W 532 run lithium triborate laser and fiber delivery system in living dogs. J Urol. 2011; 185:712–718. [PubMed: 21168876]
11. Jacques SL. Laser-tissue interactions. Photochemical, photothermal, and photomechanical. Surg Clin North Am. 1992; 72:531–558. [PubMed: 1589829]
12. Hermanns T, Sulser T, Fatzer M, et al. Laser fibre deterioration and loss of power output during photo-selective 80-w potassium-titanyl-phosphate laser vaporisation of the prostate. Eur Urol. 2009; 55:679–685. [PubMed: 18387731]
13. Hermanns T, Strebel DD, Hefermehl LJ, et al. Lithium triborate laser vaporization of the prostate using the 120 W, high performance system laser: high performance all the way? J Urol. 2011; 185:2241–2247. [PubMed: 21497852]
14. Farag E, Baccala AA Jr, Doutt RF, et al. Laser bladder perforation from photoselective vaporization of prostate resulting in rhabdomyolysis induced acute renal failure. Minerva Anestesiol. 2008; 74:277–280. [PubMed: 18327155]
15. Korossis S, Bolland F, Ingham E, et al. Review: tissue engineering of the urinary bladder: considering structure-function relationships and the role of mechanotransduction. Tissue Eng. 2006; 12:635–644. [PubMed: 16674279]

16. Thomsen S. Pathologic analysis of photothermal and photomechanical effects of laser-tissue interactions. Photochem Photo-biol. 1991; 53:825–835.

17. Kang HW, Kim J, Peng YS. In vitro investigation of wavelength-dependent tissue ablation: laser prostatectomy between 532 nm and 2.01 μm. Lasers Surg Med. 2010; 42:237–244. [PubMed: 20333741]

18. Tzortzis V, Gravas S, de la Rosette J. Minimally invasive surgical treatments for benign prostatic hyperplasia. Eur Urol Suppl. 2009; 8:489–534.

19. Rajababu K, Muir GH. Greenlight photoselective vaporization of prostate—a technical review. Prostate Cancer P Dis. 2007; 10:S6–S9.

20. Muir G, Gomez Sancha F, Bachmann A, et al. Techniques and training with GreenLight HPS 120-W laser therapy of the prostate: position paper. Eur Urol Suppl. 2008; 7:370–377.

21. Choi B, Tabatabaei S, Bachmann A, et al. GreenLight HPS 120-W laser for benign prostatic hyperplasia: comparative complications and technical recommendations. Eur Urol Suppl. 2008; 7:384–392.

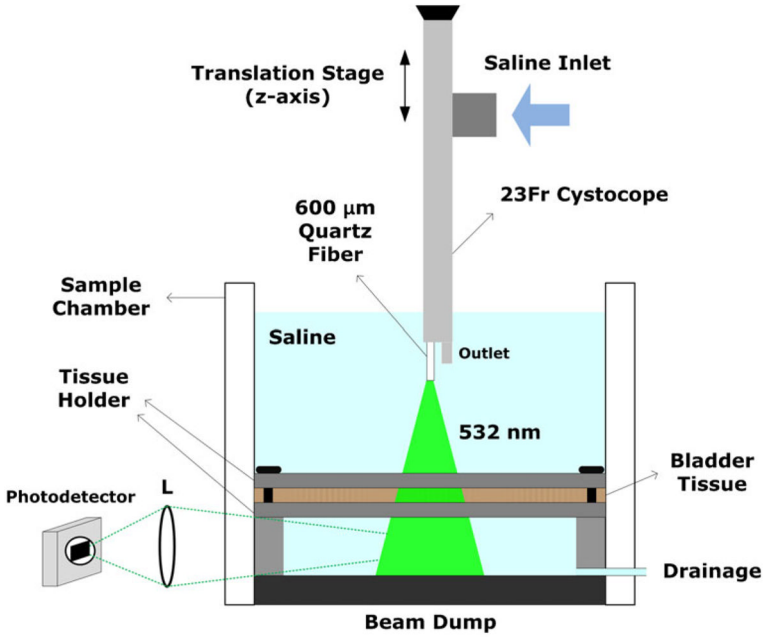

Fig. 1.

Experimental setup of the photothermal tests on bovine urinary bladder wall placed between tissue holder plates. Light (532 nm) was incident perpendicularly on the tissue surface, and a photodetector selectively collected through a lens (*L*) any scattering photons penetrating through the tissue (no unscattered transmitted light was detected). Note that a 23 Fr cystoscope was positioned along the *z*-axis to vary the physical distances between the fiber tip and the bladder tissue surface

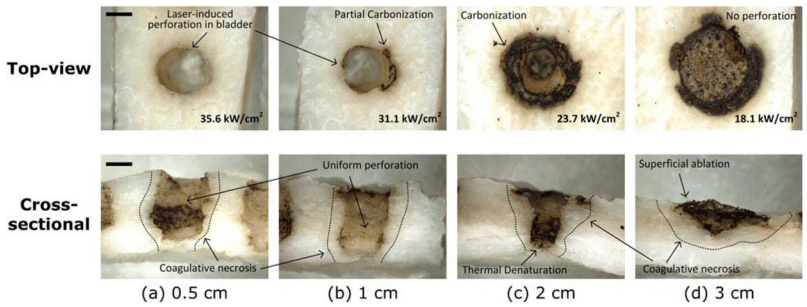

Fig. 2.

Top and cross-sectional images of laser-induced perforation in bovine bladder tissue with 120 W at various physical distances: **a** 0.5, **b** 1, **c** 2, and **d** 3 cm. The applied irradiance (kW/cm^2) at each distance is shown in top-view images (*bottom right corner*). Tissue at each distance was irradiated until perforation occurred, and its corresponding perforation time was recorded. No perforation ensued from the 3-cm condition (ablation depth=1.3 mm), and *dotted lines* (cross-sectional images) represent coagulative necrosis. *Bar*= 1.5 mm

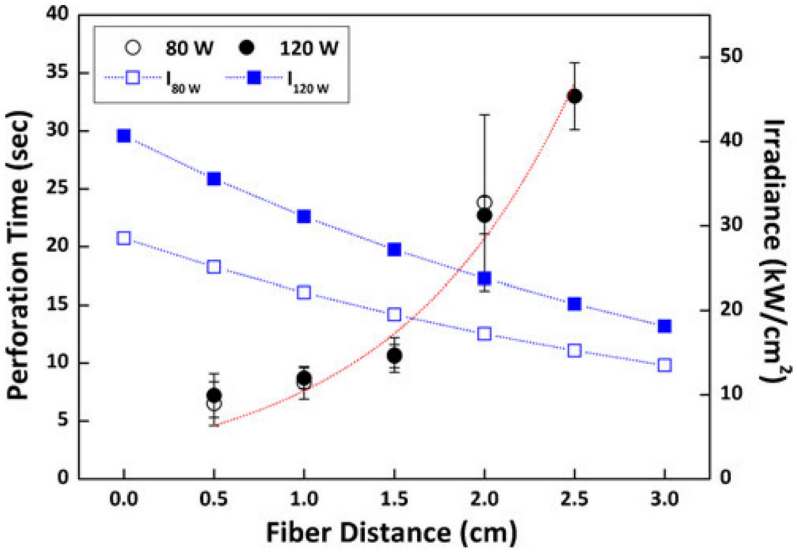

Fig. 3.

Bladder perforation time (*left axis*, N=10) and calculated irradiances (I, kW/cm^2) as a function of fiber distance between the fiber tip and the bladder tissue at 80 and 120 W. Note that *black circles* (*hollow* for 80 W and *solid* for 120 W) represent perforation time data, and *blue squares* (*hollow* for I at 80 W ($I_{80\ w}$), and *solid* for I at 120 W ($I_{120\ w}$)) represent irradiance data *Dotted lines* (*red* for perforation time and *blue* for irradiance) present the tendency of the measured data at various fiber distances. Tissue perforation occurred up to 2.0 mm at 80 W and 2.5 mm at 120 W

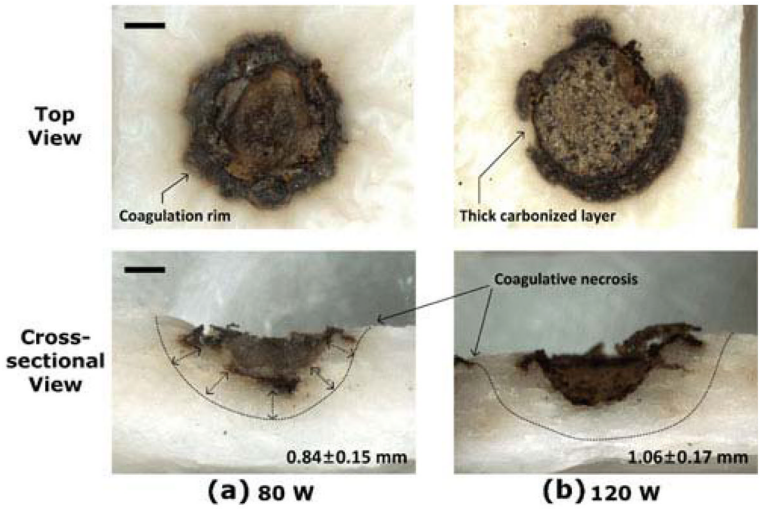

Fig. 4.

Top and cross-sectional images of the bladder tissue after 1-min irradiation with **a** 80 and **b** 120 W at a fiber distance of 3 cm from the tissue. Note that no perforation occurred for both cases. Measured thermal coagulation is shown in cross-sectional images (*bottom right corner*). Statistical significance existed between the two groups ($p < 0.005$, $N=6$)

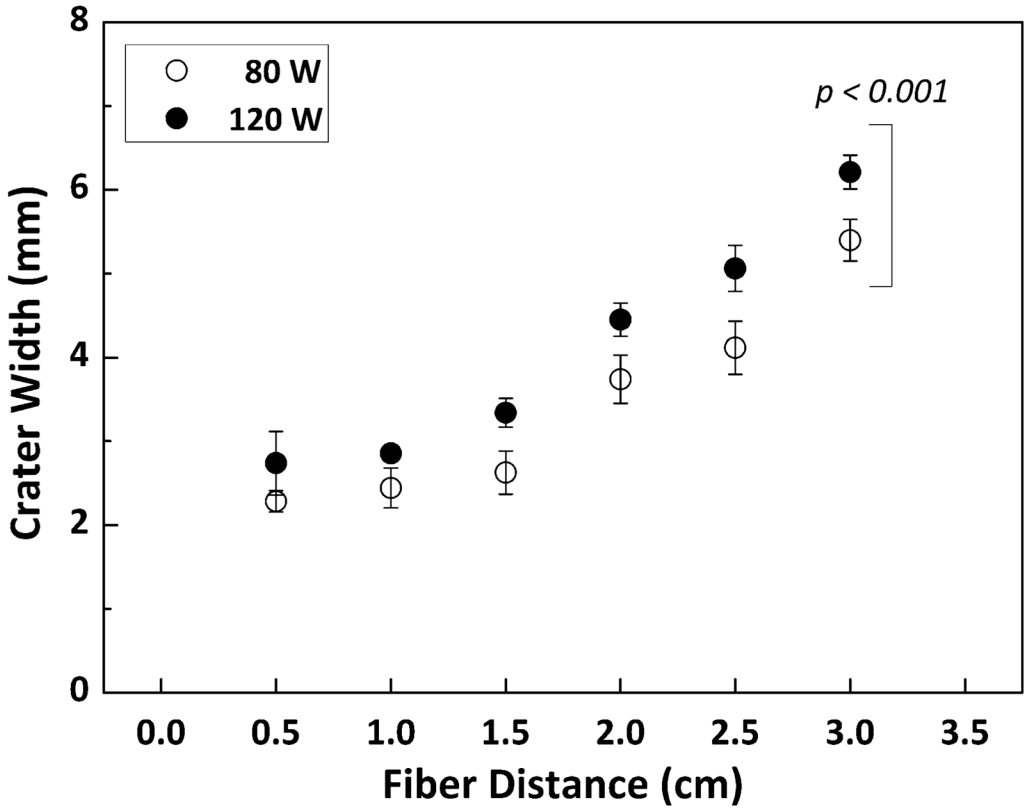

Fig. 5.
Comparison of ablated crater width as a function of fiber distance at 80 W (*hollow circle*) and 120 W (*solid circle*). Note that there was a statistical significance between the two groups ($p<0.001$, $N=5$)

Table 1

Comparison of perforation speed as a function of fiber distance at 80 and 120 W

	Fiber distance (cm)				
	0.5	**1**	**1.5**	**2**	**2.5**
Perforation speed (mm/s)					
80 W	0.74±0.19[a]	0.55±0.09	0.43±0.06	0.21±0.07	N/A
120 W	0.70±0.07	0.52±0.06	0.43 ±0.04	0.20±0.02	0.14±0.01
p value	0.63	0.47	0.88	0.76	N/A

[a]Mean±1 SD

Lasers Med Sci. Author manuscript; available in PMC 2014 September 01.